

A broadband cavity ring-down spectrometer based on an incoherent near infrared light source

Katharina Salfner · Michael Böhm ·
Oliver Reich · Hans-Gerd Löhmannsröben

Received: 14 October 2013 / Accepted: 5 January 2014 / Published online: 12 February 2014
© Springer-Verlag Berlin Heidelberg 2014

Abstract We report on the development of a cavity ring-down (CRD) spectrometer based on an incoherent broadband light source centered at 1,545 nm. One measurement spans over 46 nm. Due to the challenge of broadband CRD spectroscopy in the addressed spectral range, an extended measurement principle is developed. First successful measurements in the spectral range between 1,547 and 1,593 nm of a cavity filled with CO₂ are shown. In order to compare the experimentally determined data to values of the HITRAN database, the calculation of the expected values is discussed under consideration of the spectrometer's spectral resolution. Comparison with the data based on the HITRAN database shows good agreement.

1 Introduction

Cavity ring-down (CRD) spectroscopy, a highly sensitive technique for measuring absolute values [1] of very low absorbances, has been in active development since first being reported in 1988 by O'Keefe and Deacon [2]. Today, CRD spectroscopy is widely used for manifold applications such as the investigation of atmospheric gases [3, 4], isotope ratios [5, 6], processes on surfaces [7, 8], or investigation of very small liquid sample volumes [9]. In one of the first papers on broadband CRD spectroscopy, Engeln and Meijer [10] use a dye laser in the visible spectral range as light source and combine the CRD setup with a Fourier Transform spectrometer to scan across the dye laser spectrum. Therefore, this might be designated to be the first

broadband approach to CRD spectroscopy. Ball and Jones [11] provide an overview of the challenges of broadband CRD spectroscopy and its development until 2003. Stelmaszczyk et al. [12] report on the development of a broadband CRD spectrometer for the visible spectral range based on a white-light supercontinuum source, hence the name supercontinuum CRD spectroscopy. A possible limiting factor to the broadband approach in CRD spectroscopy is the restricted high-reflectivity bandwidth of the mirrors. This can be solved using prisms instead like has been done by Johnston and Lehmann [13].

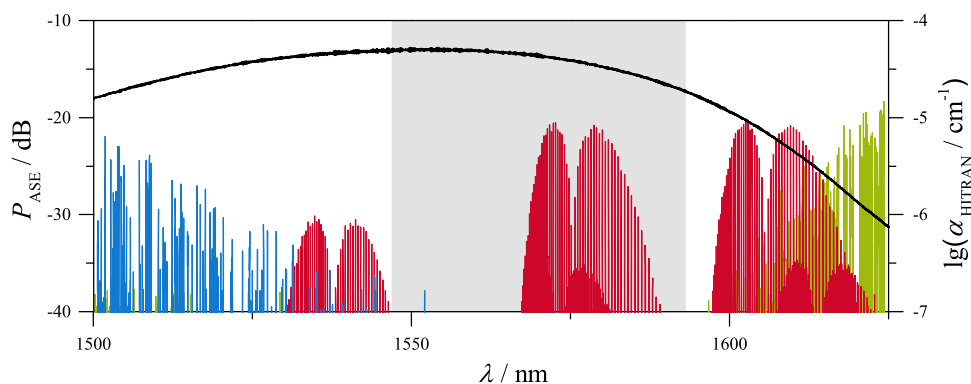
The spectrometer presented here is intended for the measurement of gases. As many gases absorb in the near infrared (NIR) spectral range broadband CRD spectroscopy in the NIR is useful for investigating gases and is the focus of this paper. Figure 1 shows the emission spectrum of the NIR light source used here and absorption signals for CO₂, CH₄, and H₂O. These three gases are the main components of biogas, which could be a target gas of the spectrometer presented here. The emission spectrum of the light source was measured with an optical spectrum analyzer (Yokogawa, AQ6370), whereas the data for the gases are taken from the HITRAN database [14]. Figure 1 illustrates that the use of broadband light sources in the NIR range allows for simultaneously detecting gases in atmospheric studies.

The use of an incoherent light source for CRD spectroscopy has been reported before [15, 16]. One advantage of incoherent light sources is that they do not exhibit a longitudinal mode structure. Therefore, mode-matching procedures like Pound–Drever–Hall laser frequency stabilization [17, 18] or “dynamic” coupling schemes [19] used for coherent light sources are not necessary.

In our setup, we combine the spectrally broadband approach with CRD spectroscopy using an incoherent light

K. Salfner · M. Böhm · O. Reich (✉) · H.-G. Löhmannsröben
Department of Chemistry, innoFSPEC Potsdam, University of
Potsdam, Am Mühlenberg 3, 14476 Potsdam, Germany
e-mail: oreich@uni-potsdam.de

Fig. 1 Comparison of the experimentally determined emission spectrum of the light source (black) and the absorption signals of CO₂ (red), CH₄ (green), and H₂O (blue), based on the HITRAN database [14]. The concentration of the gases is 1 % in N₂ each at a total pressure of 1,013 hPa and at 298 K. The gray area illustrates the spectral range of the measurement shown in Fig. 5



source that emits in the NIR spectral region. As mentioned above, broadband CRD spectroscopy in the visible range has already been demonstrated [11, 12]. Transferring this technique to the NIR requires significant changes of the measurement principle, mainly because of the insufficient detection rate of InGaAs photodiode arrays.

We first give a brief introduction to the basics of CRD spectroscopy. In Sect. 3, the setup and the developed measurement principle of the broadband CRD spectrometer are presented. Section 4 shows the results of the measurements and gives a detailed description of the algorithm that modifies values taken from the HITRAN database to the specific experimental settings, in particular the spectral resolution of the presented setup.

2 Definition of cavity ring-down parameters

In conventional CRD spectroscopy, as invented by O’Keefe and Deacon [2], the decay of the intensity of a light pulse within a cavity is measured. The time-dependent signal decays exponentially, following:

$$P(t) = P_0 \exp\left(-\frac{t}{\tau}\right). \quad (1)$$

The ring-down time τ is defined as the duration after which the power P has decreased to $1/e$ of its initial value P_0 . τ depends on the reflectivity of the cavity mirrors R and various losses V . If there is an absorbing species present, τ additionally depends on the absorption of that species, which is given by the Lambert–Beer law as (αL) . The symbol α represents the absorption coefficient of the species and L represents the length of the cavity, which is completely filled with the sample. Summarizing these dependencies gives

$$\tau = \frac{L}{c(\alpha L - \ln(R) - \ln(1 - V))}. \quad (2)$$

For gases, the speed of light in the medium c can be assumed to be of the same value as the speed of light in vacuum c_0 . Typical values for the reflectivity of the mirrors R used for CRD spectroscopy are 0.999 and higher. The

term $(1 - V)$ is also close to 1. Under these assumptions, Eq. 2 can be simplified to

$$\tau = \frac{L}{c(1 - R + V + \alpha L)}. \quad (3)$$

If there is no absorbing sample present inside the cavity, Eq. 3 is simplified to

$$\tau_0 = \frac{L}{c(1 - R + V)}. \quad (4)$$

The ring-down time of the empty cavity is called τ_0 . By measuring the ring-down time of the empty (τ_0) and the filled cavity (τ), the absolute absorber concentration $[A]$ can be calculated from

$$\alpha = \frac{1}{c} \left(\frac{1}{\tau} - \frac{1}{\tau_0} \right) = \varepsilon[A] = \sigma N. \quad (5)$$

The extinction coefficient ε and the absorption cross section σ of an absorber are available in databases such as HITRAN [14]. Therefore, the absorber concentration $[A]$ and the number density N are determined by measuring the two time constants τ and τ_0 .

Applying these equations to the broadband approach requires consideration of the wavelength dependence of R , V , and α . The resulting wavelength dependency for τ and τ_0 is addressed below.

3 The broadband cavity ring-down spectrometer

3.1 The experimental setup

The experimental setup is given in Fig. 2. An amplified spontaneous emission (ASE) diode serves as an incoherent broadband light source. A high beam quality is achieved by coupling the light source to a single-mode fiber, which works as a spatial mode filter [20]. To match the beam to the TEM₀₀ cavity mode, two lenses are used. The crucial component of the CRD spectrometer is a cavity formed with high-reflectivity mirrors. After transmission through the cavity, the broadband emission is diffracted by a

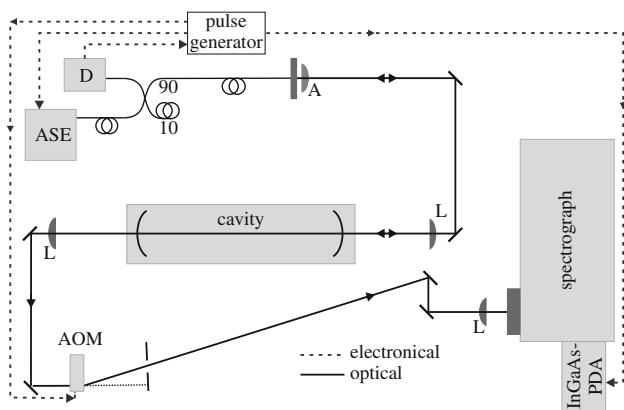


Fig. 2 Experimental setup of the broadband CRD spectrometer. ASE-amplified spontaneous emission diode, *D* InGaAs photodiode, AOM acousto-optical modulator, *A* aspheric lens, *L* lens, InGaAs PDA InGaAs photodiode array

grating spectrometer, which uses an InGaAs photodiode array (InGaAs PDA) as a detector.

The bandwidth (3 dB) of the ASE diode (DenseLight Semiconductors, DL-ASE-IM-CSC107A) is 70 nm, the center wavelength of the emission is 1,545 nm, and the total output power of the ASE diode is about 10 mW. This power of the ASE diode emission can be modulated with a frequency of up to 200 MHz and is therefore much faster than a ring-down event, which is very important for an optimal signal processing [21]. The fiber of the ASE diode is coupled to a 90:10 fiber coupler (Thorlabs, 10202A-90-FC). One of the fibers is connected with an InGaAs photodiode (Terahertz Technologies Inc., TIA-5251-FC). Behind the 90 % fiber of the coupler the beam is collimated by an aspheric lens ($f = 8$ mm) and then mode-matched to the cavity's fundamental spatial mode by an additional lens ($f = 8$ mm).

The cavity is built up of two identical plano-concave mirrors (Layertec) at a distance of 0.5 m. The reflectivity R of the mirrors is 0.9999 between 1,450 and 1,670 nm, specified by Layertec, and the minimum transmission is specified as 0.001 % for each mirror. The radius of curvature is 1 m. To check the value of $R - V$ experimentally, the ring-down time of the empty cavity was measured. Figure 3 gives the determined ring-down times in the range of 1,546–1,593 nm measured with the broadband CRD spectrometer presented here and following the measurement principle explained later. The ring-down time appears to be independent of the wavelength in the considered spectral range and the averaged value of τ_0 is (9.2 ± 0.6) μ s. Following Eq. 4, this results in a value of $R - V$ of 0.99982 ± 0.00001 and therefore in a Q factor of about 1.7×10^4 . In Fig. 3, the noise increases toward longer wavelengths because of the lower emission power of the ASE diode.

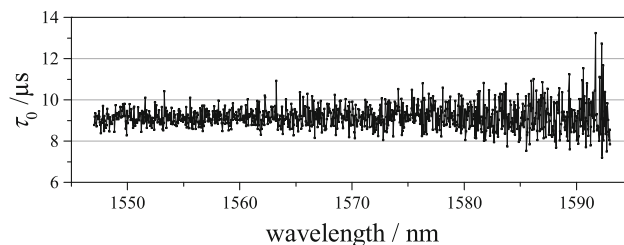


Fig. 3 Experimentally determined ring-down times of the empty cavity

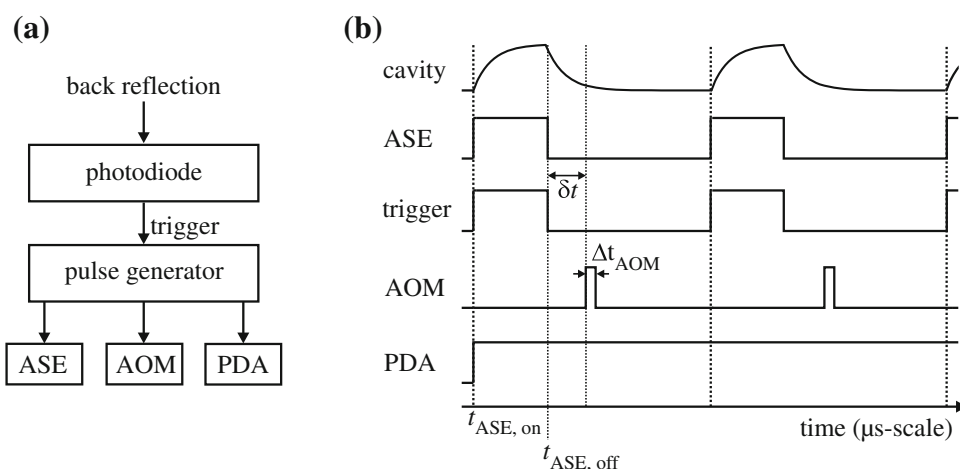
After the cavity, the beam is again collimated and passes through an acousto-optical modulator (AOM; Isomet, 1205C-2-NIR), which is used as a switch. The tuning bandwidth of the AOM is 30 MHz, and the diffraction efficiency at 1,550 nm is above 25 %. The first-order diffraction behind the AOM is passed on to the spectrograph (Andor Technology, SR-750), which has a focal length of 0.75 m and is equipped with a grating of 600 l/mm. The InGaAs PDA (Andor Technology, iDus InGaAs 491) has $1 \times 1,024$ pixels and a maximum detection rate of 193 spectra/s. It can be cooled down to 203 K without the need of liquid nitrogen. In combination with the SR-750 spectrograph, a spectral resolution of about 0.1 nm is achieved.

As mentioned above, the beam was carefully matched to the spatial modes of the cavity by a two lens system. The beam parameters were determined using a monochromatic laser (1,600 nm) coupled to the single-mode fiber and following the knife-edge method [22]. To verify whether no higher spatial modes are excited, the mode structure was measured using the monochromatic laser and varying the cavity length via a piezo element attached to one of the cavity mirrors. In the case of broadband excitation of a cavity, the wavelength dependence of the beam parameters has to be considered.

3.2 The measurement principle of the broadband cavity ring-down spectrometer

As in conventional CRD spectroscopy, the cavity is filled up with the radiation of the light source. After a certain time, the light source is switched off and the ring-down event takes place. The maximum detection rate of the InGaAs PDA is too low to detect the microsecond ring-down events. Therefore, we extended the conventional CRD technique by a time-gated sampling technique, which is used to improve the temporal resolution of the system. The AOM is used for the gating of this sampling technique. A pulse generator (Stanford Research Systems, DG645) manages the trigger cascade of the sampled measurement. The pulse generator is connected to the photodiode, the AOM, the ASE diode, and the InGaAs PDA. Figure 4a

Fig. 4 Scheme of the trigger cascade. **a** Connection scheme of the electronic devices. **b** Temporal scheme of the trigger cascade. Two trigger cycles are given. At the top, the cavity signal is shown



gives the connection scheme of the components involved in the trigger cascade.

Figure 4b shows the temporal trigger scheme of the broadband CRD spectrometer. At the beginning of each trigger cycle, the ASE diode, the AOM, and the InGaAs PDA are off. The first trigger cycle starts with switching on the ASE diode ($t_{\text{ASE, on}}$). On a nanosecond timescale, the back reflection of the first cavity mirror impinges on the photodiode, which is coupled to a 90:10 fiber coupler. The signal of this photodiode serves as the trigger for the pulse generator. When the pulse generator receives the signal from the photodiode, it immediately passes on a signal to the InGaAs PDA to start the exposition. After a certain time $t_{\text{ASE, off}}$, the ASE diode is switched off and the ring-down event takes place. After the time period δt the AOM is switched on to start the gating. From this moment, the light transmitted through the cavity is passed on to the spectrograph and the InGaAs PDA for the duration of Δt_{AOM} . At the time $t_{\text{ASE, on}}$, the ASE is switched on again and the trigger cycle starts again. The InGaAs PDA is programmed to be active for 1–2 s. During this time, the trigger cycle is constantly repeated and the signal of the chosen time gate is integrated on the InGaAs PDA. Afterward, the value of δt is changed, and the next time gate will be detected. As a result, the integrated signal power P is recorded simultaneously for all wavelengths as function of δt . By this, the ring-down signal is scanned temporally and afterward reconstructed. Therefore, we propose to call this extended technique “reconstructed cavity ring-down spectroscopy.”

As in conventional CRD spectroscopy, the information is taken from the temporal decay of the intensity after the light source is switched off. Due to the sampling technique, the initial amplitude of the ring-down signal can vary according to fluctuations of the intensity of the ASE diode. The output stability of the ASE diode used for this setup is

specified by the supplier to be 0.05 dB. Therefore, the systematic error can be estimated to be in the range of 1 %. The random error is significantly reduced by averaging over several ten thousand signals within 1–2 s.

4 Results and discussion

Figure 5 gives an exemplary reconstructed broadband CRD signal of the cavity filled with a CO₂–N₂ mixture with a CO₂ concentration of 1.1 % at a total pressure of 1,010 hPa and at room temperature. The center wavelength of the spectrometer was set to 1,570 nm, and a spectral bandwidth of 46 nm was detected simultaneously. The temporal gate of the sampling was set to $\Delta t_{\text{AOM}} = 5 \mu\text{s}$ and the total trigger cycle duration to 55 μs . The ASE diode was switched on for 15 μs . The InGaAs PDA exposition time was set to 2 s; therefore, the signals of over 36,000 trigger cycles were added up on the InGaAs PDA. Each measurement was repeated 20 times. The gate was then shifted by 1 μs , so that the temporal gates (Δt_{AOM}) were overlapping.

The data of the twenty measurements by the InGaAs PDA are averaged for each particular pixel. The resulting averaged broadband CRD signal is given as a 3D graph in Fig. 5a. The measured power (z -axis) is given in terms of counts on the InGaAs PDA; the spectral domain (x -axis) is given in terms of pixel, and the temporal domain is given as δt . The two graphs in Fig. 5b, c are slices of the 3D graph. Figure 5b gives the power as function of wavelength at the very start of the ring-down signal. The absorption of CO₂ is already visible between pixel 400 and pixel 900, but the signal is rather noisy and the baseline is overlain by the emission of the ASE diode. Figure 5c gives the power as function of time for the pixel 1. The curve exhibits the expected exponential decay.

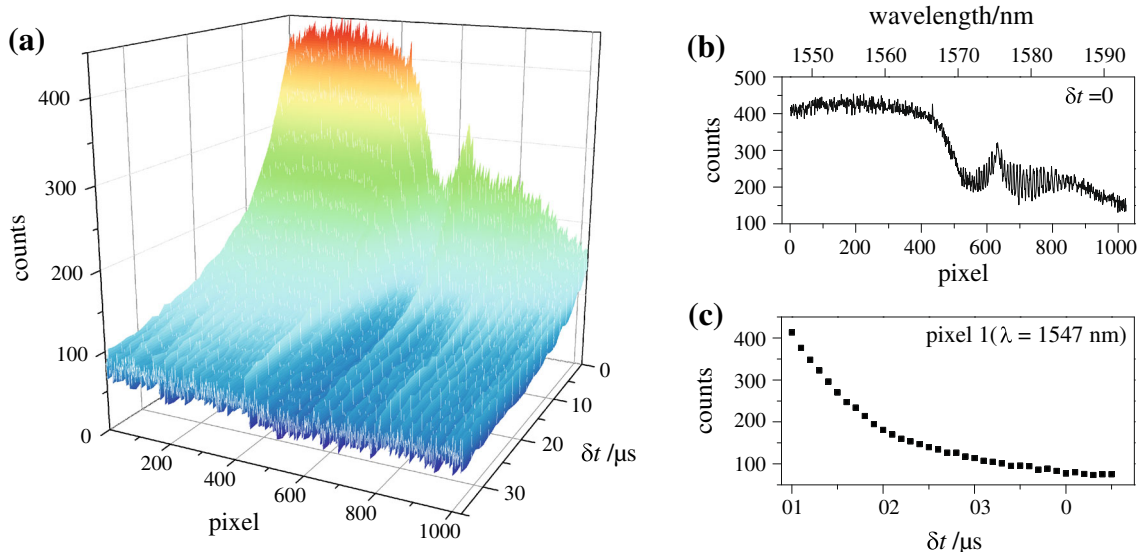


Fig. 5 **a** Experimentally determined broadband CRD signal. δt represents the time passed after shutting off the ASE diode. **b** and **c** Slices of the 3D graph given on the left

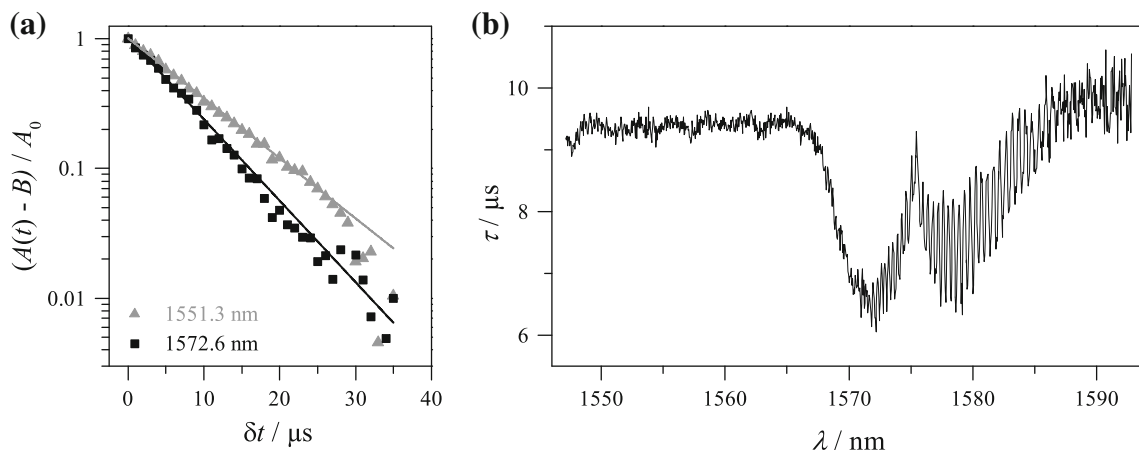


Fig. 6 **a** Exponential decays of the background-corrected normalized signal of two different pixels, i.e., at two different wavelengths. *Triangles* and *squares* show the experimental values, the lines show

mono-exponential fits. **b** Resulting ring-down times for all wavelengths λ . The cavity was filled with a CO₂-N₂ mixture with a CO₂ concentration of 1.1 % at a total pressure of 1,010 hPa

A mono-exponential curve (Eq. 6) was fitted to the ring-down signal of each pixel. The parameter A_0 is the initial amplitude of the decaying signal and B is the background.

$$A(t) = A_0 \exp\left(-\frac{t}{\tau}\right) + B \tag{6}$$

Equation 6 was fitted to the experimental data following the nonlinear least-squares Marquardt–Levenberg algorithm. The background offset of the broadband CRD signal in Fig. 5 is around 70 counts. The overlaying noise is about 3 counts. With the maximum signal of about 450 counts, this results in an actual signal-to-noise ratio (SNR) of about 150. Figure 6a shows exemplary ring-down signals of two different pixels, i.e., two different wavelengths. For better

visualization, the signals are background-corrected and normalized. Ring-down times of $(9.4 \pm 0.2) \mu\text{s}$ (triangles) and $(6.9 \pm 0.2) \mu\text{s}$ (squares) are calculated. For broadband ring-down signals, mono-exponential decays are an approximation (cf. [11]). Figure 6a shows that the assumption of mono-exponential decays seems applicable as a first approximation. Figure 6b gives the calculated ring-down times τ for all wavelengths λ . The *P* and *R* bands of the vibrational signal of CO₂ and many of the rotational bands are clearly visible.

To evaluate the qualitative and quantitative accuracy of the experimentally determined data, expected values for the absorption coefficient $\alpha(\lambda)$ based on the HITRAN database [14] are calculated for comparison. First, the

experimental values of $\alpha(\lambda)$ are calculated following Eq. 5. The value of τ_0 is taken from the baseline of the spectrum in Fig. 6b, i.e., the average of the ring-down times in the spectral range between 1,547 and 1,560 nm. Second, to calculate expected values of $\alpha(\lambda)$, the known measurement parameters (concentration of CO₂, total pressure, temperature) are entered into the information system HITRAN on the web [23]. This gives the expected values of $\alpha(\lambda)$ with a spectral resolution of about 2 pm, which are not directly comparable to our experimentally determined data, as the spectral resolution of the broadband CRD spectrometer is about 0.1 nm. This resolution is not sufficient to resolve the particular absorption lines as these exhibit a bandwidth of about 65 pm. A higher spectral resolution could be achieved using another grating. However, the drawback would be that the spectral bandwidth of the measurement would be decreased, which contradicts the broadband approach.

Therefore, for broadband CRD spectroscopy, the strong wavelength dependency on the sub-nanometer scale of both, the absorption coefficient $\alpha(\lambda)$ and the resulting ring-down time $\tau(\lambda)$, has to be considered. As a consequence of the spectral resolution of the spectrometer, the spectral bandwidth of the absorbance signal and the wavelength dependency of the ring-down time $\tau(\lambda)$, the ring-down signal detected by a particular pixels is

$$P(t, \lambda) = \frac{P_0}{\Delta\lambda} \int \exp\left(-\frac{t}{\tau(\lambda)}\right) d\lambda \quad (7)$$

with $\delta\lambda$ representing the wavelength range of the light that hits the pixel. For the comparison of the experimentally determined and expected values of $\alpha(\lambda)$, this wavelength dependency has to be taken into account. Therefore, the expected values of $\alpha(\lambda)$ have to be calculated under consideration of the instrument function of the broadband CRD spectrometer, which mainly accounts for the spectral resolution of the spectrometer.

This algorithm is implemented as follows: firstly, expected ring-down signals $P_j(t)$ are calculated for each pixel j under consideration of the effective spectral resolution $\delta\lambda_s$ and using values of α taken from HITRAN. Secondly, the simulated ring-down signals $P_j(t)$ are analyzed in the same way as the experimental data, i.e., a mono-exponential function (Eq. 6) is fitted to $P_j(t)$. Thirdly, from the resulting values of $\tau(\lambda)$, the expected values of the absorption coefficient $\alpha(\lambda)$ are calculated and compared to the experimentally determined values.

The expected ring-down signal $P_j(t)$ is a sum of all exponential decay signals of the wavelengths that hit the particular pixel j . For this summation, the different initial values for the particular wavelengths depending on the absorption have to be considered. Furthermore, the effective spectral resolution, especially the cross talk is relevant.

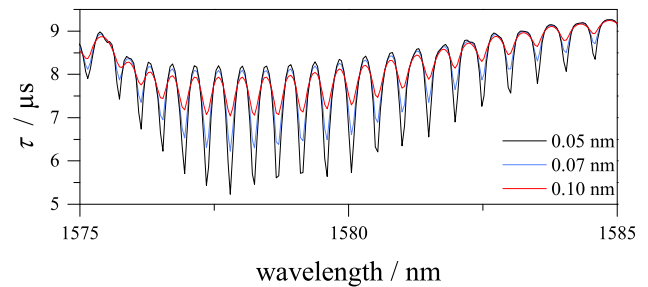


Fig. 7 Expected ring-down times for different assumed effective spectral resolutions $\delta\lambda_s$

For the calculation of $P_j(t)$, values of α are used, which are given by the information system HITRAN on the web [23] with a spectral resolution of 2 pm. HITRAN on the web delivers a number of $\lambda_i - \alpha_i$ data pairs M , which are used to calculate expected ring-down signals $P_j(t)$ for each pixel j following the equation

$$P_j(t) \propto \sum_{i=1}^M \underbrace{\exp(-c\alpha_i \Delta t_{ASE})}_{\text{term A}} \times \underbrace{\exp\left[-t\left(c\alpha_i + \frac{1}{\tau_0}\right)\right]}_{\text{term B}} \times \underbrace{\frac{\delta\lambda_p}{2\pi\delta\lambda_s} \times \exp\left[-\frac{(\lambda_i - \lambda_j)^2}{2\delta\lambda_s^2}\right]}_{\text{term C}} \quad (8)$$

with these parameters: Δt_{ASE} , the time span during which the broadband light source is switched on and the cavity is filled with light; $\delta\lambda_p$, the ratio of the spectral bandwidth of the measurement to the number of pixels; and λ_j , representing the central wavelength of the light hitting on the particular pixel j .

The value of $\delta\lambda_s$ has to be calibrated by the measurement of a known gas at known measurement parameters (concentration, total pressure, temperature) and depends on the width of the entrance slit of the spectrograph. For the measurement shown here, a value of $\delta\lambda_s = 0.07$ nm was determined. The value of $\tau_0 = 9.4$ μ s is taken from the experimental data. All parameters are given by the experimental settings or the HITRAN database. Therefore, Eq. 8 contains no fit parameters.

Term A is a weighting factor which considers the stronger influence of signals caused by low α_i to the total ring-down signal on that pixel. Term B represents the temporal decay of the ring-down signal. The term C is a rescaled point spread function (PSF) which represents the contribution of α_i to the signal detected by pixel j (cross talk). For this PSF, a Gaussian shape is assumed.

Figure 7 gives the expected ring-down times for three different assumed effective spectral resolutions $\delta\lambda_s$ calculated following the algorithm discussed above. This figure illustrates the influence of $\delta\lambda_s$ on the spectrum. The

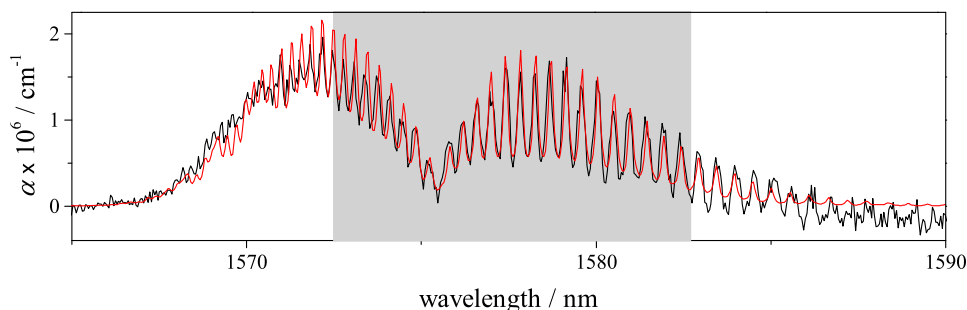


Fig. 8 Experimentally determined absorption coefficient $\alpha(\lambda)$ (black) in comparison with expected values of $\alpha(\lambda)$ based on the HITRAN database (red). The data from HITRAN are calculated under

consideration of the instrument function of the broadband CRD spectrometer. The gray area depicts the spectral range considered for the more detailed quantitative comparison given in Fig. 9

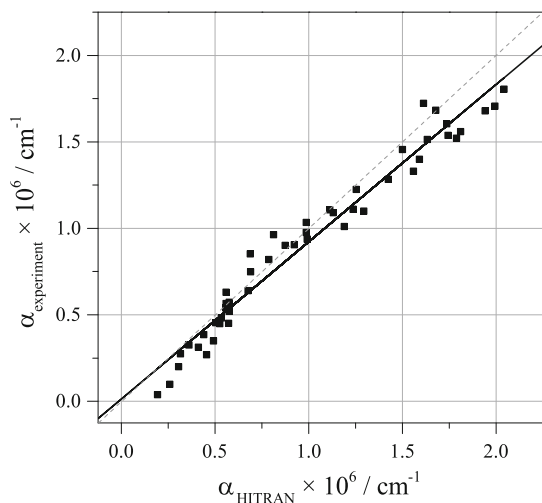


Fig. 9 Quantitative comparison of the experimentally determined absorption coefficients ($\alpha_{\text{experiment}}$) and the expected values (α_{HITRAN}). The black squares are the corresponding α values for the minima and maxima of the particular rotational signals in Fig. 8 between 1,572.4 and 1,582.8 nm (gray area). The dashed gray 1:1 line gives the values for the case that experimental and expected data perfectly agree. The solid black line gives the linear fit to the data

contrast of the particular rotational signals and the mean of the signals vary with $\delta\lambda_S$.

Figure 8 gives the comparison of the experimentally determined absorption coefficients $\alpha(\lambda)$ and the expected values based on the HITRAN database. The two spectra are qualitatively and quantitatively in good agreement. For α above 1,583 nm, some of the experimentally determined values are seemingly negative. This artifact is caused by measurement errors mainly by the lower spectral power density of the light source. The limit of detection is estimated from the standard deviation of the α values in the range, where no absorption by CO_2 is detected (1,546–1,564 nm). The value of α_{LOD} is estimated to $1.5 \times 10^{-7} \text{ cm}^{-1}$.

A closer look at the quantitative agreement between the experimentally determined and the expected values of $\alpha(\lambda)$ is given in Fig. 9. This graph compares the corresponding maximum and minimum α values of the particular

rotational signals in Fig. 8 between 1,572.4 and 1,582.8 nm (gray area). The dashed gray 1:1 line in Fig. 9 represents the case that experimentally determined and expected values are in perfect agreement. The solid black line gives the linear fit of the depicted values. The intercept of the fit is at $(1.4 \pm 2.9) \times 10^{-8} \text{ cm}^{-1}$ and the slope is 0.91 ± 0.03 . The deviation of the slope from the value 1 indicates a slight systematic error.

5 Conclusion

In this paper, we present the first results of a broadband CRD spectrometer based on an incoherent NIR source. Due to the insufficient detection rate of the InGaAs PDA, an extended measurement principle is developed; we suggest calling this technique “reconstructed CRD spectroscopy.” This technique offers the possibility to combine the high sensitivity of CRD spectroscopy with a broadband approach and therefore the possibility to detect different species of a gas mixture simultaneously. Using an NIR light source, the spectrometer works in a spectral range which is of high interest for gas sensing. NIR broadband ring-down signals are presented. The comparison of the experimentally determined absorption coefficients to expected values of the absorption coefficients based on the HITRAN database shows qualitatively and quantitatively good agreement.

Monochromatic state of the art CRD spectrometers achieve sensitivities of up to 10^{-12} cm^{-1} , special variants even 10^{-14} cm^{-1} [24]. In comparison, the sensitivity of the spectrometer presented here ($\alpha_{\text{LOD}} \approx 10^{-7} \text{ cm}^{-1}$) is rather low but close to detection limits of other broadband approaches of CRD spectroscopy in the visible spectral range ($0.6 \times 10^{-7} \text{ cm}^{-1}$ [25]). This loss in detection sensitivity is a trade-off for the benefit of the decrease in cross sensitivity, to name only one of the advantages of broadband approaches. These promising results presented here show that the high potential of NIR broadband CRD

spectroscopy can be exploited with the presented spectrometer.

Acknowledgments We acknowledge the financial support of the German Federal Ministry of Education and Research (Grant No. 03Z2AN12). K. Salfner thanks the UP Transfer GmbH for the financial support.

References

1. D. Romanini, A.A. Kachanov, F. Stoeckel, *Chem. Phys. Lett.* **270**, 546–550 (1997)
2. A. O’Keefe, D.A.G. Deacon, *Rev. Sci. Instrum.* **59**, 2544–2551 (1988)
3. H. Chen, A. Karion, C.W. Rella, J. Winderlich, C. Gerbig, A. Filges, T. Newberger, C. Sweeney, P.P. Tans, *Atmos. Meas. Tech.* **6**, 1031–1040 (2013)
4. R.A. Washenfelder, N.L. Wagner, W.P. Dube, S. Brown, *Environ. Sci. Technol.* **45**, 2938–2944 (2011)
5. N.C. Munksgaard, K. Davies, C.M. Wurster, A.M. Bass, M.I. Bird, *Isot. Environ. Health Stud.* **49**, 232–242 (2013)
6. D. Balslev-Clausen, T.W. Dahl, N. Saad, M.T. Rosing, *J. Anal. At. Spectrom.* **28**, 516–523 (2013)
7. M. Thämer, A. Kartouzian, P. Heister, S. Gerlach, M. Tschurl, U. Boesl, U. Heiz, *J. Phys. Chem.* **116**, 8642–8648 (2012)
8. H.V. Powell, M.A. O’Connell, M. Zhang, S.R. Mackenzie, P.R. Unwin, *Anal. Chem.* **84**, 2585–2591 (2012)
9. H. Waechter, D. Munzke, A. Jang, H.-P. Looock, *Anal. Chem.* **83**, 2719–2725 (2011)
10. R. Engeln, G. Meijer, *Rev. Sci. Instrum.* **67**, 2708–2713 (1996)
11. S.M. Ball, R.L. Jones, *Chem. Rev.* **103**, 5239–5262 (2003)
12. K. Stelmaszczyk, M. Fechner, P. Rohwetter, M. Queier, A. Czyżewski, T. Stacewicz, L. Wöste, *Appl. Phys. B* **94**, 369–373 (2009)
13. P.S. Johnston, K.K. Lehmann, *Opt. Express* **16**, 15013–15023 (2008)
14. L.S. Rothman, C.P. Rinsland, A. Goldman, S.T. Massie, D.P. Edwards, J.-M. Flaud, A. Perrin, C. Camy-Peyret, V. Dana, J.-Y. Mandin, J. Schroeder, A. McCann, R.R. Gamache, R.B. Wattson, K. Yoshino, K.V. Chance, K.W. Jucks, L.R. Brown, V. Nemtchinov, P. Varanasi, *J. Quant. Spectrosc. Radiat. Transf.* **60**, 665–710 (1998)
15. S.M. Ball, J.M. Langridge, R.L. Jones, *Chem. Phys. Lett.* **398**, 68–74 (2004)
16. I. Ventrillard-Courtillot, E. Sciamma O’Brien, S. Kassi, G. Méjean, D. Romanini, *Appl. Phys. B* **101**, 661–669 (2010)
17. R.W.P. Drever, J.L. Hall, F.V. Kowalski, J. Hough, G.M. Ford, A.J. Munley, H. Ward, *Appl. Phys. B* **31**, 97–105 (1983)
18. A. Foltynowicz, P. Maślowski, A.J. Fleisher, B.J. Bjork, J. Ye, *Appl. Phys. B* **110**, 163–175 (2013)
19. R. Grilli, G. Méjean, C. Abd Alrahman, I. Ventrillard, S. Kassi, D. Romanini, *Phys. Rev. A* **85**, 051804 (2012)
20. O. Wallner, W.R. Leeb, P.J. Winzer, *J. Opt. Soc. Am. A* **19**, 2445–2448 (2002)
21. K.K. Lehmann, H. Huang, in *Optimal Signal Processing in Cavity Ring-Down Spectroscopy*, ed. by J. Laane *Frontiers in Molecular Spectroscopy* (Elsevier, Amsterdam, 2009)
22. N. Hodgson, H. Weber, *Laser Resonators and Beam Propagation* (Springer, New York, 2005)
23. HITRAN on the web, <http://hitran.iao.ru> (2013) [June 2013]
24. G. Berden, R. Engeln, *Cavity Ring-Down Spectroscopy* (Wiley, New York, 2009)
25. W.M. Nakaema, Z.-Q. Hao, P. Rohwetter, L. Wöste, K. Stelmaszczyk, *Sensors* **11**, 1620–1640 (2011)